Article

Synthesis, Spectroscopic and Nonlinear Optical Properties, and Antimicrobial Activity of Cu(II), Co(II), and Ni(II) Complexes: Experimental and Theoretical Studies

Riaz Hussain,* Syed Laila Rubab, Afifa Maryam, Tuba Ashraf, Muhammad Arshad, Kiran Lal, Sajjad H. Sumrra, Shafaq Ashraf, and Bakhat Ali*

Cite This: ACS Omega 2023, 8, 42598−42609

Read Online

ACCESS | Metrics & More | Article Recommendations | SI Supporting Information

ABSTRACT: Currently, we report the preparation of transition metal complexes Co(II), Ni(II), and Cu(II) of hydrazone Schiff base ligands, which are obtained by the condensation reaction of substituted salicylaldehyde and hydrazines. The synthesized hydrazone ligands and their metal complexes were characterized by spectroscopic methods such as Fourier transform infrared (FT-IR), UV−vis, nuclear magnetic resonance (^1H NMR and C^{13} NMR), and mass spectrometry analyses. All of the quantum chemistry calculations were performed using DFT executed in the Gaussian 09 software package. The geometry was optimized by using the density functional theory (DFT) approximation at the B3LYP level with a basis set of 6-31G (d, p). There was excellent agreement between the FT-IR values obtained experimentally and those obtained theoretically for the test compounds. It is worth noting that none of the optimized geometries for any of the Schiff base and metal complexes had any eigenvalues that were negative, indicating that these geometries represent the true minimum feasible energy surfaces. We also analyzed the electrostatic potential of the molecule and NBO calculation at the same level of theory. Gauss View 6 was utilized for the file organization of the input data. Gauss View 6.0, Avogadro, and Chemcraft were used to determine the data. Additionally, synthesized compounds were screened for antimicrobial activity against Gram-negative bacteria (*Salmonella typhi*, *Escherichia coli*) and Gram-positive bacteria (*Bacillus halodurans*, *Micrococcus luteus*) and two fungal strains (*Aspergillus flavus*, *Aspergillus niger*). These research findings have established the potential of ligands and their metal complexes as antimicrobial agents. Additionally, the compounds demonstrated promising nonlinear optical (NLO) properties, with potential applications across a wide range of contemporary technologies.
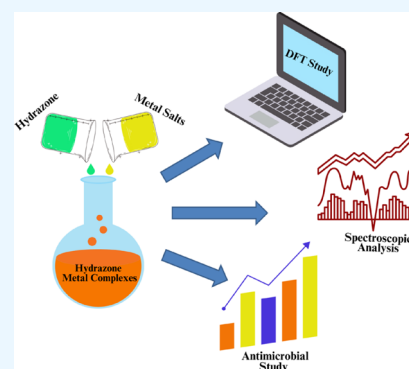
1. INTRODUCTION

The study of hydrazone molecules and their metal complexes has garnered significant interest within the fields of organic and coordination chemistry[1] due to their remarkable coordination abilities, diverse physiological activities,[2] luminescence properties,[3] and wide range of applications in various areas such as pharmacological,[4] biological,[5] catalytic, and analytical fields of chemistry.[6] Hydrazones are a significant group of organic compounds having a broad spectrum of pharmacological activities predominantly[7] and anti-inflammatory,[8] analgesic,[9] antimicrobial,[10] antifungal,[11] anticancer,[12] and antidepressant activities.[13] Hydrazone applications in organic chemistry was first established by Emil Fischer in 1884 and proved to be a Schiff base-type compound.[14] Hydrazones contain an azomethine group (−C=N-NH−) and are considered as an important class of organic compounds having two nitrogen species that are different in nature.[15] Notably, hydrazones with the azomethine group have gained significant attention as key organic compounds for the development of novel drugs. Beyond pharmaceutical applications, they find use in the fields of organic ligands, corrosion science,[16] bioactive materials,[17] catalysis,[18] chemo sensors,[19] and fluorescence signals.[20]

Furthermore, hydrazone Schiff base ligands are significant materials in bioinorganic chemistry due to the presence of N and O donor atoms that form stable metal complexes with an extensive variety of metals.[21] Transition metal complexes based on halogen and nitro groups have promising biological properties.[22] Different fragments attached with hydrazones affect the coordinating ability and show attractive coordination sites to bind to metal ions and form complexes. A vast study of metal ions revealed that the cobalt(II) complex displays usefulness in stomach ulcer and rheumatoid arthritis.[23] Copper(II) complexes are used as anticancer drugs that
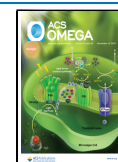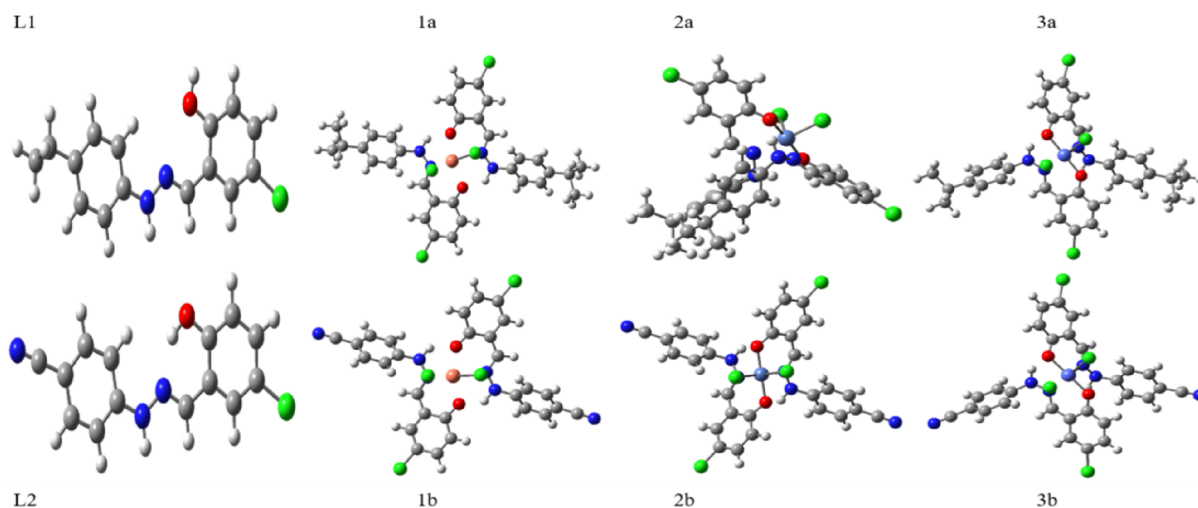
Figure 1. Optimized geometry of the synthesized molecules.

could lead to cancer cell death via different mechanisms, i.e., DNA damage and generation of reactive oxygen species (ROS).[24] Hydrazone derivatives and their transition metal complexes show remarkable thermo- and photochromic applications, which make these compounds valuable in modern technology, which includes light-emitting diodes,[25] optical computers, solar filters, and imaging systems, and also appropriate due to their nonlinear optical properties in photonic and electronic devices.[26]

Moreover, the importance of compounds that have non-linear optical (NLO) characteristics extends across other disciplines, including chemical dynamics, nuclear research, medicine, biology, and surface interface presentations.[27] NLO materials are pivotal in technologies such as optical computing, communication, and dynamic image processing. The preparation of various NLO materials, spanning inorganic and organic semiconductors, polymer architectures, and engineered nano-structures, necessitates diverse techniques.[28] Organic NLO materials offer advantages such as cost-effectiveness, low dielectric constants, substantial photoelectric coefficients, and ease of implementation. Notably, phenyl hydrazone derivatives have demonstrated potent crystalline and nonlinear optical (NLO) characteristics.[29] Consequently, exploring the NLO properties of newly synthesized compounds within this framework holds immense promise.[30]

Taking into account the role of hydrazones and their metal complexes in the biological field and possessing a comprehensive research background encompassing both synthetic and computational fields, here, we reported the synthesis of hydrazone ligands **L₁** 4-chloro-2-((4-isopropylphenyl)-hydrazono)methyl)phenol and **L₂** 4-(2-(5-chloro-2-hydroxybenzylidene) hydrazinyl)benzonitrile and their Cu(II), Ni(II), and Co(II) complexes and then studied their spectroscopic and nonlinear optical properties. The synthesized compounds were subjected to the determination of antimicrobial activity against two Gram-negative bacteria and Gram-positive bacteria and two fungal strains, wherein the complexes showed a moderate activity against pathogenic bacteria. The computations of density functional theory (DFT) provide a multitude of useful information about the compounds. The correlation between these calculations and the physicochemical properties of the compounds is strong. It is well known that the physicochemical properties of compounds also affect their

biological activity.[31,32] The purpose of the DFT calculations was to examine the relationship between theoretically obtained data and experimental data.

2. RESULTS AND DISCUSSION

The synthesized compounds were examined by FT-IR and NMR spectroscopic analysis. In the FT-IR spectrum of the ligands (**L₁** and **L₂**),absorption bands at 3388 and 3306 cm⁻¹ due to the OH group, a strong absorption band at 3306−2936 cm⁻¹ for (N−H) stretching frequencies, and an absorption band at 1665−1600 cm⁻¹ for the ν(C = N) vibrations were observed. The OH vibrations disappeared from the spectra of the complexes, which indicated the coordination of metal ions to the hydroxyl group after deprotonation. In the complexes' spectra, the azomethine bands ν(C=N) and ν(C−O) (i.e., phenolic oxygen) were shifted to lower frequencies and changes in band frequency indicate that the nitrogen atom of the azomethine group was brought into being involved in coordination with metal ions. So, it can be concluded that ligands phenolic oxygen and azomethine nitrogen were responsible for coordinating with central metal ions. Furthermore, some imperative bands appeared in complexes in ranges between 653 and 558 cm⁻¹ assigned to (M−O) and 560−541 cm⁻¹ assigned to (M−N), which gives further confirmation of complex formation. The appearance of new spectral bands suggests the presence of chemical linkages that include heteroatoms, such as azomethine nitrogen, deprotonated oxygen, and chlorine atoms. These heteroatoms are coordinated to the core metal ion. This discovery provides strong evidence for the adoption of an octahedral geometry in all of the metal complexes being studied. The main absorption bands of ligands **L₁**and **L₂** and their complexes **1a**−**3a** and **1b**−**3b** are listed in Table S1 and Figures S1−S8.

In the ¹H NMR spectra of hydrazone ligand **L₁**, a doublet appears at 1.18 ppm due to the (CH₃)₂ protons of the isopropyl group. A multiplet signal appears due to the −CH− proton of the isopropyl group at 2.80 ppm. The chemical shift of the azomethine N=CH proton in both ligands (**L₁** and **L₂**) appeared at 8.05 and 8.20 ppm. The singlet peak of NH proton appeared in both ligands at 10.40 and 10.32 ppm due to the electronegative atom attached to the proton, which in turn increases the deshielding effect of the proton. Furthermore, the singlet peak at 10.55 ppm corresponds to hydroxyl (OH)
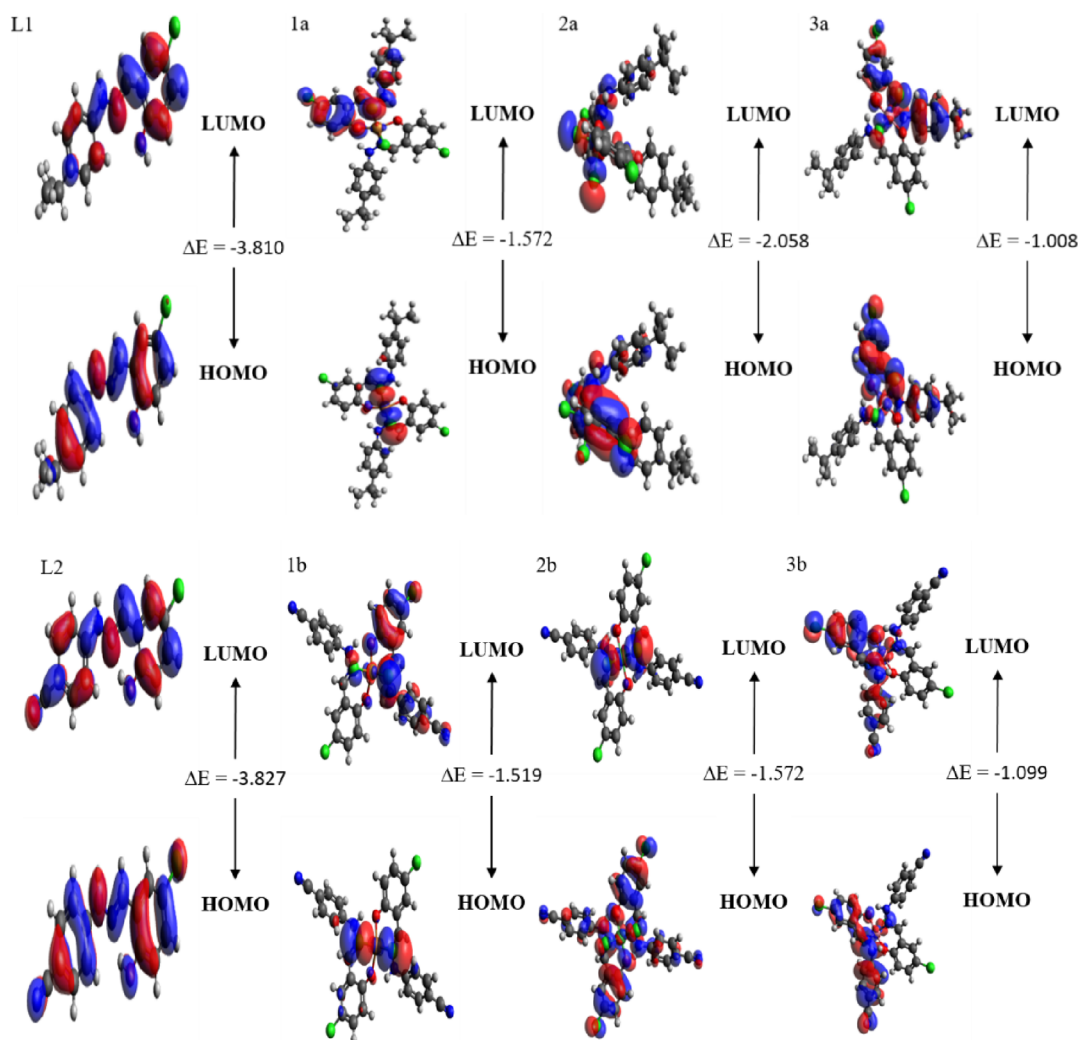
Figure 2. Frontier molecular orbital pictorial representation

protons. The aromatic protons were resonated at 6.86−7.59 and 6.88−7.72 ppm (Figures S9 and S10). In ^{13}C NMR, the peak for azomethine (C=N) carbon in L_1 and L_2 was observed at 159.2 and 157.3 ppm. In the L_1 spectra, signals appeared at 20.3 and 44.9 ppm due to the presence of methyl and methylene carbon of the isopropyl group. In the L_2 spectra, one signal appeared at 110.2 ppm to recognize the presence of cyano carbon (CN). All of the aromatic carbons in L_1 and L_2 were resonated around 120.3−131.4 and 120.3−131.4 ppm (Figures S11 and S12).

Mass spectrometry (HRMS) analysis was conducted on the synthesized ligands (L_1 and L_2) and their respective complexes (**1a−3a**, **1b−3b**) dissolved in acetonitrile. The obtained data confirmed the proposed chemical structures. The molecular ion peak for hydrazone ligands (L_1 and L_2) was detected at m/z 289.6149 and 272.7118, consistent with their calculated value. Similarly, the molecular ion peaks for their **1a−3a**, **1b**, and **3b** complexes were observed at m/z 711.1009, 706.0072, 706.0078, 676.8579, 672.0049 and 672.2363, respectively. These mass spectrometry results align with the expected molecular weights, providing strong evidence of the formation of the complexes.

2.1. DFT Calculations. Hydrazone ligands and their metal complexes are optimized using DFT with B3LYP/6-31G (d, p). Figure 1 presents the optimal geometries for each structure.

2.2. Frontier Molecular Analysis. The FMO theory is presently regarded as an effective tool for determining a molecule's reactivity as well as its electrical and optical properties. This is useful for investigating how excited-state lowest unoccupied and highest occupied molecular orbital energies are corelated to one another.[33] The B3LYP/6-311G (d, p) level of theory is used to calculate the frontier molecular orbitals of molecules. The visual representation is illustrated in Figure 2, and the energy band gap is given in Table. 1. A large energy gap indicates that the structure is thermodynamically stable. A small energy gap in a structure indicates it is more

Table 1. Energy Band Gap Calculation

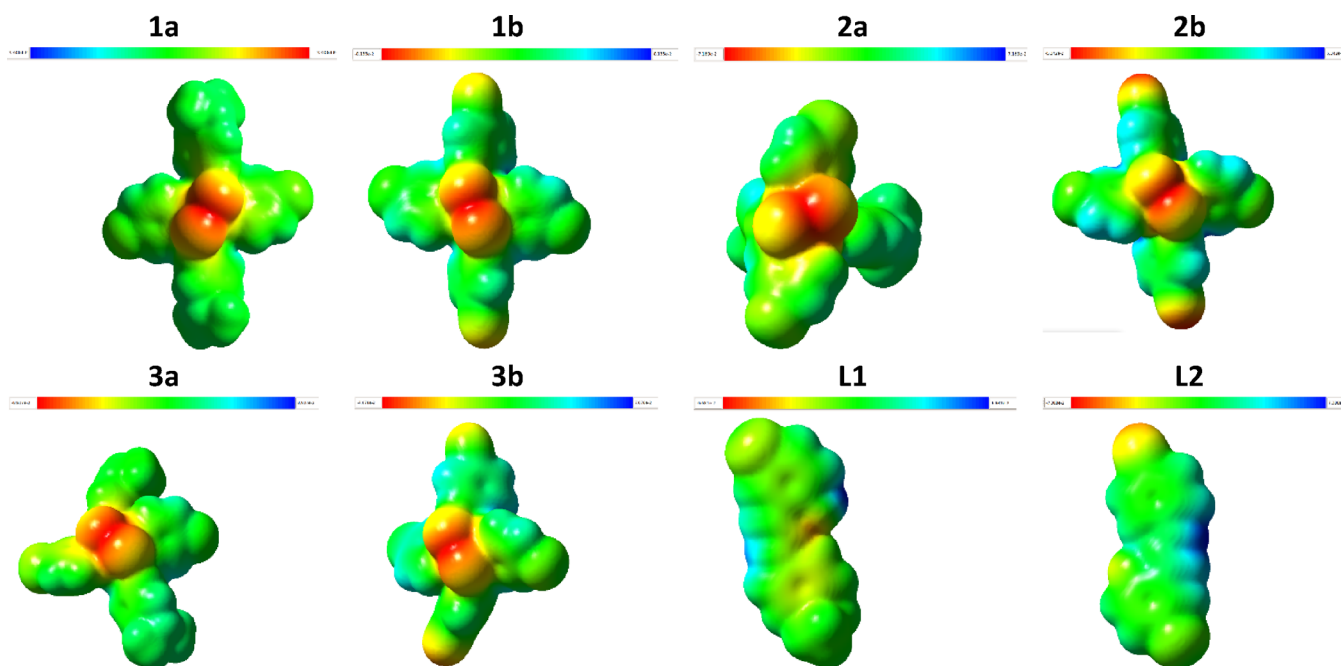| complex	HOMO (ev)	LUMO (ev)	energy band gap
L1	−5.0069121	−1.19724	3.81
1a	−5.5086645	−3.936743	1.57
2a	−5.8289262	−3.770762	2.06
3a	−5.6047158	−4.596585	1.01
L2	−5.8215795	−1.995037	3.83
1b	−6.2661909	−4.746785	1.52
2b	−6.3320391	−4.440128	1.89
3b	−6.2272806	−5.128269	1.10

Figure 3. Molecular electrostatic potential of the compounds at the DFT/B3LYP/6-31G (d, p) basis set.

reactive and more polar.[34] Red indicates the negative part, and blue indicates the positive part.

The energy difference between ligand 1 and its complexes is given as **L1 > 2a > 1a > 3a**. Energy difference between ligand 2 and its complexes is given L2 > 2b > 1b > 3b. The order in metal complexes shows nickel metal complex are more stable and cobalt metal complex are more reactive.

2.3. Molecular Electrostatic Potential. The investigation of the three-dimensional plot of electron density on the entire compound is conducted by the study of molecule electrostatic potential, employing eq 1

$$V(r) = \sum \left(\frac{Z_A}{R_A} - r \right) - \int (p(\overrightarrow{r'})/\overrightarrow{r'} - r) \mathrm{d}\overrightarrow{r'} \tag{1}$$

The equation shown above introduces the variable $V(r)$ that denotes the molecular electrostatic potential. Additionally, Z_A is used to indicate the charge density over the nucleus. The electronic density function is defined as $p(r')$ at a certain location denoted as R_A, where r' represents the integration variable.[35,36] The color observed in MEP (molecular electrostatic potential) analysis serves to delineate the regions inside a molecule that are susceptible to electrophilic and nucleophilic attack. The magnitude of electrostatic potential increases in the following order: red < orange < yellow < green < blue.[37] The red hue signifies the optimal location for electrophilic attack, whereas the blue hue designates the spot most conducive to nucleophilic attack. The MEP analysis was conducted using the B3LYP/6-31G (d, p) basis set. The obtained results are depicted in Figure 3. The observation reveals that oxygen atoms exhibit a negative potential, as indicated by the red hue, whereas the positive potential is predominantly displayed in the blue area by nitrogen atoms, with hydrogen and carbon atoms partly contributing. The green area represents the mean potential, which refers to the range between the two extremes. The presence of distinct reaction sites in all molecules can be inferred from the observation of red and blue colors.

2.4. Global Reactivity Parameters. The HOMO and LUMO orbital energies are used in the equations to generate global reactivity descriptors.[38] The stability, selectivity, and reactivity of the species are all heavily dependent on these global reactivity factors.[39,40] Tabulated reactivity parameters and their corresponding computed values are listed in Table 2.

Table 2. X (Electronegativity), EA (Electron Affinity), IP (Ionization Potential), μ (Chemical Potential), S (Global Softness), η (Global Hardness), and ω (Global Electrophilicity) of Schiff Base Ligands and Metal Complexes

Sr. no.	X	EA	IP	μ	S	H	ω
L1	3.102	1.197	5.007	−3.102	0.262	1.905	2.526
1a	4.723	3.937	5.509	−4.723	0.636	0.786	14.189
2a	4.800	3.771	5.829	−4.800	0.486	1.029	11.194
3a	5.101	4.597	5.605	−5.101	0.992	0.504	25.807
L2	3.908	1.995	5.822	−3.908	0.262	1.913	3.992
1b	5.506	4.747	6.266	−5.506	0.658	0.760	19.956
2b	5.386	4.440	6.332	−5.386	0.529	0.946	15.334
3b	5.678	5.128	6.227	−5.678	0.910	0.550	29.333

Global hardness follows the same order as energy band gap, whereas global softness follows the opposite order. Others parameters also depend on the energy band gap.

2.5. NBO Analysis. Gaussian 09W software was used to do NBO analysis[41] on complexes at the B3LYP/6-311G (d, p) level of theory. Natural bond orbital (NBO) studies are useful for understanding the charge relocation between full and unoccupied orbitals.[42] NBO data helps us understand intermolecular delocalization and the charge concentrations that shift in D-π-A structures from donor to acceptor regions.[43]

There were typically three distinct types of electronic transitions detected. Among these, σ-σ* transitions were more prominent. Other transitions include σ-π*, L.P-σ*, and L.P-π*. For calculating the relationships between the donor and

Table 3. Dipole Moment (μ) and Linear Polarizability (α) of Hydrazone Ligands and Metal Complexes

	μ_x	μ_y	μ_z	μ	α_{xx}	α_{yy}	α_{zz}	α_{total} (au)
1a	0.367	0.329	−3.331	−3.331	1200.440	982.644	323.865	835.65
2a	−2.318	−3.179	0.868	0.868	668.160	569.450	443.746	560.45
3a	−1.722	−2.453	−3.235	−3.235	708.465	689.426	332.826	576.91
1b	0.008	−0.304	−3.733	−3.733	732.357	779.327	287.008	599.56
2b	0.001	−0.001	−2.117	−2.117	676.505	653.824	305.455	545.26
3b	−1.374	−1.250	−3.350	−3.350	664.491	674.163	289.007	542.55
L1	−0.387	0.323	−0.0002	−0.0002	434.922	197.410	88.872	240.40
L2	1.351	−1.367	0.002	0.002	431.597	176.213	61.101	222.97

Table 4. Hyperpolarizability (β) of Hydrazone Ligands and Metal Complexes

	β_{xxx}	β_{xxy}	β_{xyy}	β_{yyy}	β_{xxz}	β_{yyz}	β_{xzz}	β_{yzz}	B_{zzz}	β_{tot} (au)
L1	3852.232	957.641	48.87	−32.41	−0.58	0.003	−8.09	14.90	−0.02	4,004.93
1a	1684.642	−661.254	35.50	2136.75	969.62	2556.27	−129.77	291.21	−2489.33	2,593.26
2a	1259.788	−186.598	1908.83	1951.09	125.78	−2183.75	1293.19	2909.22	−2849.16	8,113.65
3a	−17905.436	−6153.474	2218.10	−31249.65	11500.47	6.36	−1556.81	−1657.11	−328.51	44,136.00
L2	−48.292	523.968	−33.08	−92.50	−1.13	0.12	12.11	−2.26	0.003	434.76
1b	−3869.642	−5327.854	−507.62	−1622.18	−2072.04	−1028.69	−670.23	−1837.15	−2951.58	11,803.49
2b	6.495	−4.333	0.10	1.101	4153.70	985.50	1.80	−0.62	679.36	5,818.57
3b	671.930	−3901.290	5197.21	−54863.01	4662.1	1757.39	−39.26	−1661.66	−741.75	60,971.48

acceptor, a second-order perturbation model study of the Fock matrix was performed[44] and stabilization energy was calculated using eq 2

$$E^2 = q_i \frac{(F_{ij}^2)}{\varepsilon_i - \varepsilon_j} \tag{2}$$

All types of vibrations in structures and their stabilization energies are given in the table. The charge transfer characteristics found by NBO analysis of these compounds are significant for their possible NLO features. Natural bond orbital analysis with second-order perturbation study for hydrazone ligands and metal complexes using B3LYP/6-311G (d,p) is presented in Table S2.

2.6. NLO Properties. Optical switches, communication technology, signal processing, and optical memory devices all make substantial use of NLO compounds. The optical response, which is related to both the nonlinear (hyper polarizabilities) and linear (polarizability, etc.) responses (Table 3), is caused by the electrical properties of the entire compound.

Dipole moment comparisons describe the directional distribution of charges in the molecules that we have analyzed. The highest dipole moment is 0.868 au, and the lowest value is −3.733 au. The findings of the polarizability tensors in the x, y, and z directions show that the x-axis polarizability tensor is the most important and has a significant impact on the overall linear polarizability values (Table 4). The average polarizability values for the ligands are 240.40 and 222.97 au. The maximum polarizability value is 835.65 au, and the minimum value is 222.97 au, and the ligands have a minimum polarizability value.

Table 4 shows the values of β_{tot} and its nine contributing tensors in the x, y, and z axes. The maximum hyperpolarizability value is 60,971.48 au, while the minimum value is 434.76 au.

2.7. FT-IR Calculations. Molecular vibrations obtained by modern vibrational spectroscopy have sparked the interest of both the computational and experimental communities. On the optimized geometries of molecules, we estimated the theoretical vibrational spectra of the synthesized compounds using DFT at the B3LYP/6-31G (d, p) level of theory. The vibrational modes in the investigated compounds were assigned using the animation feature of Gauss-View. The experimental and computed harmonic vibrational frequencies for all compounds are given below (Table 5).

At the optimized geometry for the compounds, all calculated harmonic-vibrational frequencies were found to be active, and no imaginary frequency modes were generated. It is clear that the practical FT-IR results and the corresponding theoretically simulated results had a good correlation.

2.8. ADMET Properties. Swiss ADMET was used to forecast the results of ADMET investigations of isolated substances (1a−3a, 1b−3b, L1, and L2) to predict the absorption, distribution, metabolism, excretion, and toxicity (ADMET) features to assess the bioavailability of the compounds. The skin's ability to absorb molecules is measured by its permeability (Kp) in cm/s. The skin permeability, Kp, values of all compounds varied from 1.59 to −5.45 cm/s in silico, indicating low skin permeability. Additionally, the blood-brain barrier (BBB) and gastrointestinal (GI) permeability show how medication molecules are absorbed and distributed.[45,46] The findings of the in silico predictions for the chemicals (1a−3a, 1b−3b, L1, and L2) under study's absorption, distribution, metabolism, and excretion (ADME) are shown in Table 6. According to the Swiss ADME prediction parameters, the complexes showed low GI absorption, whereas L1 and L2 showed high GI absorption. The blood-brain barrier (BBB) permeability of L1 and L2 was similarly demonstrated by Swiss ADME prediction, but not those of the complexes. Additionally, a variety of cytochromes (CYPs) control how drugs are metabolized, with CYP1A2, CYP2C9, CYP2C19, CYP3A4, and CYP2D6 being particularly important for the biotransformation of drug compounds.[47]

Thus, complexes (1a−3a) inhibit CYP2D6 and the permeability glycoprotein (P-gp) substrate, according to in silico Swiss ADME prediction. The permeability glycoprotein (P-gp) substrate and CYP2C19 were both suppressed by complexes 1b−3b. A substrate of the permeability glycoprotein (P-gp) was inhibited by ligand 1 along with all cytochromes

Table 5. Compound Vibrational Frequencies Measured Experimentally and Those Anticipated by Applying the B3LYP and 6-31G (d, p) Theory[a]

			computed vibrational frequencies of hydrazone ligands and metal complexes		
compound		$I_{IR(Experimental)}$	$I_{IR(DFT)}$	I_{IR}	vibrational assignments
L1	O−H	3306	3808	42.8031	vO−H
	N−H	3034	3491	0.9106	vN−H
	C=N	1666	1674	8.2848	v(as)C=N+ v(as)C=C$_{Ben}$ + w=C−H
	M−N				
	M−O				
L2	O−H	3388	3473	298.5587	v(as)O−H(dominant) + v(as)N−H
	N−H	3306	3534	11.2259	v(s)N−H(dominant) + v(s)0−H
	C=N	1613	1619	12.1413	v(s)C=N + v(s)C=C$_{Ben}$ + w=C−H
			1665	418.9174	v(s)C=N + v(s)C=C$_{Ben}$ + w=C−H
			1668	86.2428	v(as)C=N(dominant) + w=C−H + w N−H,C−H
	C−O	1421	1524	132.0829	v(as)C−O(dominant), δ=C−H$_{Ben}$
	M−N				
	M−O				
1a	O−H				
	N−H	2960	3338	620.4916	v(as)N−H
			3395	368.5948	v(s)N−H
	C=N	1613	1589	31.5764	v(s)C=N,v(s)C=O + ρ N−H + v(s)C=C$_{Ben}$
			1607	240.531	v(s)C=N,v(s)C=O + ρ N−H + v(s)C=C$_{Ben}$
	C−O	1478	1467	4.9073	v(as)C−O+ w C−H
			1459	34.2534	v(as)C−O+ w C−H + ρ N−H
	M−N	541			
	M−O	646			
2a	O−H				
	N−H	2957	3463	130.4400	v N−H
			3456	23.9188	
	C=N	1617	1672	141.8411	v(s) C=N + ρ N−H
	C−O	1403	1322	40.4788	v(C=O)C−O + δ C−H$_{Ben}$
	M−N	565	568	9.4103	M−N
	M−O	652	635	12.7529	M−O
3a	O−H				
	N−H	2936	3557	4.7798	vN−H
			3216	681.7372	v(s) N−H
			3219	11.1900	v(as) N−H + v(as)C − H
	C=N	1617	1596	209.3973	v(s) C=N,C=O + ρ N−H
	C−O	1441	1408	146.5092	v(s)(C=O) C−O + δ=C−H
	M−N	555	513		
			548	29.9612	
	M−O	653	574	5.1099	M−O
			594	20.1169	
1b	O−H				
	N−H	3263	3387	557.25	v(s)N−H
			3479	312.120365	v(as)N−H
	C=N	1605	1583	19.7697	v(s)C=N,C=N(dominant)
			1614	88.8604	v(as)C=N,C=N, τ N−H,N−H, v(s)C=N,C=O
			1629	118.7978	v(as)C=N + w=C−H, v(as)C=C$_{Ben}$
	C−O	1425	1405	167.7398	v(s)C−O(C=O) + δ=C−H+ ρ N−H,C−H
	M−N	542	489	9.6811	M−N
			491	9.6822	
	M−O	628	641	53.2220	M−O, v N−H
2b	O−H				
	N−H	3296	3430	205.7878	v(as)N−H
			3429	5.6590	v(s)N−H
	C=N	1613	1668	133.4592	v(as)C=N + τ N−H
			1671	0.1608	v(s)C=N + τ N−H
	C−O	1286	1323	221.9161	v(as)(C=O)C−O + δ=C−H + ρ N−H
	M−N	542	542	22.8447	M−N
	M−O	557	557	6.8383	M−O

Table 5. continued

		computed vibrational frequencies of hydrazone ligands and metal complexes			
compound		$I_{IR(Experimental)}$	$I_{IR(DFT)}$	I_{IR}	vibrational assignments
3b	O−H				
	N−H	3242	3567	9.3425	vN−H
	C=N	1600	1616	15.0824	$v(s)C{=}N + v(s)C{=}C_{Ben} + \delta{=}C{-}H_{Ben} + \rho\,N{-}H$
	C−O	1202	1363	231.0465	$v(as)(C{=}O)C{-}O + \delta{=}C{-}H + \rho\,N{-}H$
	M−N	541	499 544	35.3357 18.9247	M−N
	M−O	589	579 626	15.5231 28.9156	M−O

[a]s, symmetric; v, stretching; δ, rocking; w, scissoring; ρ, wagging; as, asymmetric; τ, twisting; Exp, experimental; Theo, theoretical: Ben, benzene ring.

Table 6. ADME Predictions of Compounds 1a−3a, 1b−3b, L1, and L2 Computed by SwissADME and PreADMET

	GI absorption	BBB permeability	inhibitor interaction						skin permeation value (log Kp) (cm/s)
			P-gp substrate	CYP1A2 inhibitor	CYP2C19 inhibitor	CYP2C9 inhibitor	CYP2D6 inhibitor	CYP3A4 inhibitor	
1a	low	no	yes	no	no	no	yes	no	−1.62
2a	low	no	yes	no	no	no	yes	no	−1.59
3a	low	no	yes	no	no	no	yes	no	−1.59
1b	low	no	yes	no	yes	no	no	no	−3.71
2b	low	no	yes	no	yes	no	no	no	−3.68
3b	low	no	yes	no	yes	no	no	no	−3.68
L1	high	yes	no	yes	yes	yes	yes	no	−4.41
L2	high	yes	no	yes	yes	yes	no	yes	−5.45

other than CYP3A4 and a substrate of the P-gp was inhibited by ligand 2 along with all cytochromes other than CYP2D6.

2.9. In Silico Pharmacokinetics (Drug-likeness) and Toxicity Analysis. The SwissADME tool was used to predict in silico pharmacokinetic characteristics (drug-likeness qualities) based on Lipinski's rule of five[48] using the structures of isolated compounds (**1a−3a, 1b−3b, L1,** and **L2**) converted to their canonical simplified molecular-input line-entry system (SMILE). Lipinski's rule of five suggests that the drugs and/or candidates should abide by the five-parameter rule, which specifies that the hydrogen-bond donors (HBDs) should be less than 5, the hydrogen-bond acceptors (HBAs) should be less than 10, the molecular mass should be less than 500 Da, log P should not be less than 5, and the total polar surface area (TPSA) should not be greater than 140. Drug-likeness is a test that determines whether a specific organic molecule possesses characteristics that are typical of an orally active medication. The SwissADME tool confirmed that all complexes followed Lipinski's rule of five and are likely to be orally active (Table 7).[48] The bioavailability of the compounds and their hydrogen bonding potentials are closely connected to the TPSA value. As a result, the examined compounds' TPSA values were found to be between 44.62 and 114.14, which is significantly less than the limit of 140. The complexes and ligands' computed number of rotatable bonds (NRB) values are fewer than 10, indicating that the compounds are conformationally stable.[45]

2.10. Antimicrobial Activities. The synthesized hydrazone ligands (**L1** and **L2**) and their metal complexes were tested on two Gram-negative strains (*Escherichia coli* and *Salmonella*), Gram-positive strains (*Bacillus halodurans* and *Micrococcus luteus*), and fungal strains (*Aspergillus flavus* and *Aspergillus niger*) by a disc diffusion method. The test compounds (ligand/complex) were dissolved in DMSO. Azithromycin was used as a standard drug in pathogenic

Table 7. Drug-likeness Predictions of Compounds 1a−3a, 1b−3b, L1, and L2 Computed by SwissADME

complex	Mol. Wt. (g/mol)	NRB	NHA	NHD	TPSA (Å²)	log P (clog P)	Lipinski's rule of five violation
1a	721.99	11	3	2	66.56	7.12	0
2a	717.14	11	3	2	66.56	7.11	0
3a	717.38	11	3	2	66.56	7.11	0
1b	687.85	7	5	2	114.14	5.03	0
2b	683	7	5	2	114.14	5.03	0
3b	683.24	7	5	2	114.14	5.03	0
L1	288.77	5	2	2	44.62	4.10	yes
L2	271.70	3	3	2	68.41	2.88	yes

bacteria, and terbinafine was used as a standard drug in fungal strains. The antibacterial and antifungal activity results show that ligands were active toward these bacterial strains, but the complexes found moderate activity against pathogenic bacteria. The hydrazone ligand **L1** exhibits maximum inhibition of 11 mm against *E. coli* and *B. halodurans* bacterial strains and shows less activity against other bacterial strains. The hydrazone ligand **L2** shows a 15 mm zone of inhibition against the *E. coli* bacterial strain. Among all the complexes, complex **2b** shows the highest activity with 13, 18, and 14 mm inhibition zones against *E. coli*, *B. halodurans*, and *M. luteus*, respectively. Furthermore, the hydrazone ligand **L1** shows 6 mm zone of inhibition against *A. flavus*, while **L2** shows a 9 mm inhibition zone against *A. niger*. Complex **1b** shows the highest activity with a 14 mm inhibition zone against *A. niger*, and complexes **3a and 3b** show moderate activity with a 9 mm inhibition zone against *A. niger* as compared to other metal complexes but less activity as compared to the standard drug. The zones of inhibition against the tested bacterial and fungal strains are presented in Table 8 and Figure. 4. The activity of

Table 8. Inhibition Results of Synthesized Compounds against Bacterial and Fungal strains

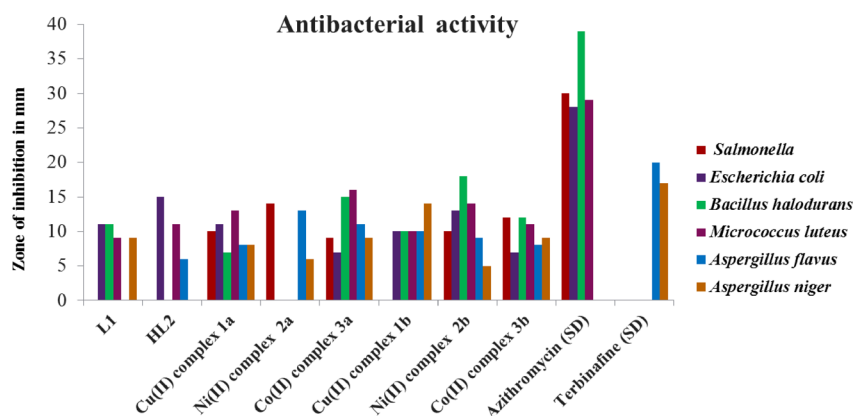|		inhibition zone (mm) antimicrobial activities					
		bacterial strains				fungal strains	
Sr.#	compounds	*Salmonella* (Gram −ve)	*Escherichia coli* (Gram −ve)	*Bacillus halodurans* (Gram +ve)	*Micrococcus luteus* (Gram +ve)	*Aspergillus flavus*	*Aspergillus niger*
1	HL$_1$		11	11	9		9
2	HL$_2$		15		11	6	
3	Cu(II) complex 1a	10	11	7	13	8	8
4	Ni(II) complex 2a	14				13	6
5	Co(II) complex 3a	9	7	15	16	11	9
6	Cu(II) complex 1b		10	10	10	10	14
7	Ni(II) complex 2b	10	13	18	14	9	5
8	Co(II) complex 3b	12	7	12	11	8	9
9	azithromycin (SD)	30	28	39	29		
10	terbinafine (SD)					20	17

Figure 4. Antimicrobial activity results of synthesized compound.

the hydrazone metal complexes is enhanced due to complexation with central metal atoms. Co(II) and Ni(II) complexes show better activity against bacteria as compared to the other compounds. Cu(II) and Ni(II) complexes show greater activity against bacterial strains, but other complexes showed better activity against fungal strains but less activity as compared to the standard drug.[49] Partial sharing between the azomethine nitrogen and phenolic oxygen with a positively charged metal atom can cause the metal to be less polar during complexation.[50] Chelation can increase the lipophilicity of metal ions[51] that enhances the permeability in lipid membranes and consequently supports the inhibition of bacterial growth by blocking the important binding sites in pathogenic bacteria.
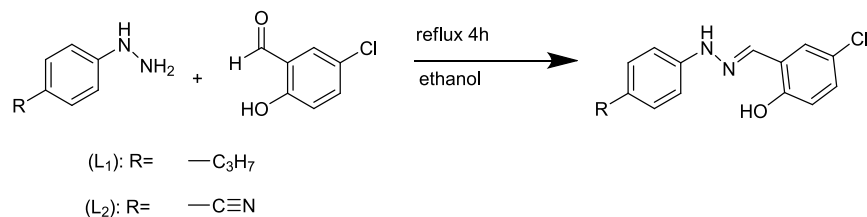
Furthermore, a comparison study was performed to assess the antibacterial activity of the recently synthesized compounds in relation to previously reported compounds and Schiff base ligands, specifically 2-(((3,4-dihydro-2*H*-benzo[*b*]-[1,4]dioxepin-7-yl)imino)methyl)-4-nitrophenol,[52] along with their corresponding metal complexes, which exhibited noteworthy antibacterial activity. Notably, the synthesized complex **2b** demonstrated an even higher effectiveness against both bacterial and fungal species. The increased effectiveness of this compound may be ascribed to the impact of substituents, such

as OH, Cl, and the azomethine group, within its molecular structure. Additionally, the compound's improved permeability properties and the intrinsic stability of the heterocyclic ring present in its structure contribute to its heightened potency.[53]
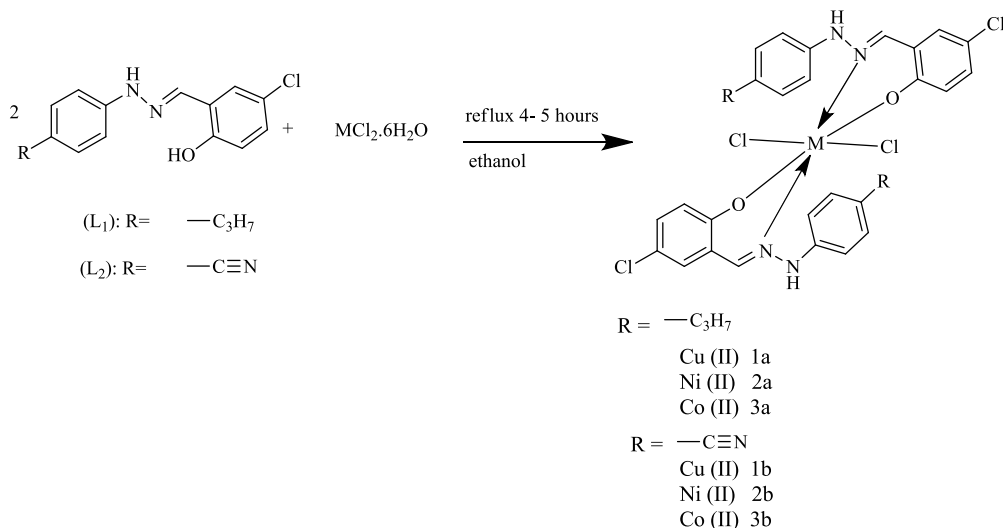
3. CONCLUSIONS

Novel hydrazone ligands and their transition metal complexes Co(II), Ni(II), and Cu(II) were synthesized and characterized by spectroscopic data (FT-IR, UV−vis, ^{1}H NMR, C^{13} NMR, and HRMS). FT-IR and HRMS analysis results show that the formation of complexes was successful and also that the complexes formed octahedral geometry. Additionally, we present the results of DFT analysis of the synthesized compounds. Resolution of the chemical structure was attained by means of NLO and IR analyses as well as NBO, FMO, and global reactivity parameters. The DFT and experimental calculations were in good agreement. FT-IR calculations were reproduced with DFT calculations. The newly prepared hydrazone ligands and their metal complexes were screened for their antimicrobial activities, and some compounds were active against Gram-negative bacteria *Salmonella* and *E. coli* and Gram-positive bacteria *B. halodurans* and *M. luteus* and show activity against *A. flavus* and *A. niger*. The results indicated that while the ligands displayed activity against the bacterial strains,

Scheme 1. Synthetic Scheme of Hydrazone Ligands

(L₁): R= —C₃H₇

(L₂): R= —C≡N

Scheme 2. Synthetic Scheme of Metal Complexes (1a−3a and 1b−3b)

(L₁): R= —C₃H₇

(L₂): R= —C≡N

R = —C₃H₇
Cu (II) 1a
Ni (II) 2a
Co (II) 3a

R = —C≡N
Cu (II) 1b
Ni (II) 2b
Co (II) 3b

the metal complexes exhibited varying degrees of effectiveness. Complex **2b**, for instance, showed the highest inhibition zones against multiple bacterial strains. The enhanced activity of the hydrazone metal complexes can be attributed to chelation with central metal atoms, leading to improved permeability and the inhibition of bacterial growth.

4. EXPERIMENTAL DETAILS

All chemicals and reagents were commercially obtained in their purest form and used without further purification.

4.1. Synthesis of Hydrazone Ligands L₁ and L₂. Schiff base ligands were synthesized according to previous literature[54] with some modifications. Ligands were synthesized by adding an ethanolic solution of 5-chlorosalicylaldehyde (0.5 g) into an ethanolic solution (10 mL) of substituted phenyl hydrazine (0.5 g) and 4-isopropyl phenyl hydrazine and 4-cyanophenyl hydrazine (0.5 g) with constant stirring and adding two drops (0.2 mL) of acetic acid to maintain the pH. The reaction mixture was refluxed at 70−80 °C for 4 h, and the completion of reaction was monitored by thin layer chromatography (TLC). A colored product was obtained, filtered, washed with ethanol, and then air-dried. Recrystallization was carried out in ethanol (Scheme 1).

4.2. Synthesis of Metal Complexes (1a−3a and 1b−3b). Metal complexes of **L₁** and **L₂** (Scheme 2) were synthesized by reacting a ligand solution with a hydrated metal(II) chloride solution in a 2:1 molar ratio. Both ligand and metal salts were dissolved in ethanol separately. Then, a hot ethanolic solution of **L₁** and **L₂** (0.1 g) was added dropwise into an ethanolic solution of hydrated metal salt (CuCl₂·6H₂O, NiCl₂·6H₂O, and CoCl₂·6H₂O) (0.03g) with constant stirring. The resulting mixture was refluxed at 70−80 °C for 4−5 h.

Reaction mixtures were kept at room temperature to evaporate the solvent, and the obtained products were recrystallized in ethanol. Reaction progress is monitored by TLC (Scheme 2).

4.3. Spectroscopic Data. All the synthesized compounds were characterized via spectroscopic techniques, and data are given below.

4.3.1. 4-Chloro-2-((2-(4-isopropylphenyl) hydrazono)-methyl)phenol (L₁). Yield, 74%; off-white crystal; M.P. 165 °C; FT-IR ν (cm⁻¹): 3033 (NH), 3305 (−OH), 1665.99 (C=N), 1588 (C−O). UV−vis (ethanol): λ_{max} 357 nm. ¹H NMR, δ(ppm): 1.16−1.18 (d, J= 5.1 Hz,6H, (CH₃)₂), 2.80 (m, J = 5.1 Hz,1H, CH-(CH₃)₂), 8.05 (s, 1H, N=CH), 10.40 (s, 1H, NH), 6.89 (d, J = 6.9 Hz, 1H, CHCH isopropyl phenyl ring), 7.59 (d, J = 7.6 Hz, 1H, CHCH isopropyl phenyl), 6.93 (d, J = 6.9 Hz, 1H, CHCH OH-phenyl), 7.16 (d, J = 7.1 Hz, 1H, CHCH OH-phenyl), 10.5 (s, CHOH-phenyl), ¹³C NMRδ (ppm): 159.2 (C=N), 20.3 ((CH₃)₂), 44.9 (CH(CH₃)₂), 120.3, 120.7, 122.4, 127.5, 127.7, 128.0, 128.1, 128.6, 130.5, 130.7, 131.4 (aromatic C and CH). HRMS (ESI): m/z [M+H]⁺ calcd. for C₁₆H₁₇ClN₂O: 289.6150, found: 289.6149.

4.3.2. 4-(2-(5-chloro-2-hydroxybenzylidene)hydrazinyl)-benzonitrile (L₂). Yield, 60%; yellow powder; M.P. 285 °C; IR ν (cm⁻¹): 3306 (NH), 3387 (−OH), 1613 (C=N), 1420 (C−O). UV−vis (ethanol): λ_{max} 358 nm. ¹H NMR, δ(ppm): 8.20 (s, 1H, N=CH), 10.32 (s, 1H, NH), 6.91(d, J = 6.9 Hz, 1H, CHCH cyano-phenyl), 7.22 (d, J = 7.2 Hz, 1H, CHCH cyano-phenyl), 7.12 (d, J = 7.1 Hz, 1H, CHCH OH-phenyl), 7.63 (d, J = 7.6 Hz, 1H, CHCH OH-phenyl), 11.03 (s, CHOH-phenyl), ¹³C NMRδ (ppm): 157.3 (C=N), 110.2 (CN−), 120.3, 120.7, 122.4, 127.5, 127.7, 128.0, 128.1, 129.1, 130.5, 130.8, 131.4 (aromatic C and CH). HRMS (ESI): m/z

$[M+ H]^+$ calculated for $C_{14}H_{10}ClN_3O$: 272.7128, found: 272.7118.

4.3.3. Bis(4-chloro-2-((E)-(2-(4 isopropylphenyl)-hydrazono)methyl)phenoxy)copper Dehydrate (1a). Yield, 70%; brown; M.P. 170 °C; FT-IR ν (cm^{-1}): 2960 (NH), 1613 (C=N), 1478 (C−O), 645 (M−O), 540 (M−N). UV−vis (ethanol): λ_{max} 361 nm. HRMS (ESI): m/z $[M+ H]^+$ calculated for $C_{32}H_{32}Cl_4CuN_4O_2$: 711.100, found: 711.1009.

4.3.4. Bis(4-chloro-2-((E)-(2-(4-isopropylphenyl)-hydrazono)methyl)phenoxy)nickel Dehydrate (2a). Yield, 69%; light orange; M.P. 172 °C; FT-IR ν (cm^{-1}): 2956 (NH), 1617 (C=N), 1402 (C−O), 651 (M−O), 564 (M−N). UV−vis (ethanol): λ_{max} 365 nm. HRMS (ESI): m/z $[M+ H]^+$ calculated for $C_{32}H_{32}Cl_4NiN_4O_2$: 706.0073, found: 706.0072.

4.3.5. Bis(4-chloro-2-((E)-(2-(4-isopropylphenyl)-hydrazono)methyl)phenoxy)cobalt Dehydrate (3a). Yield, 68%; brown; M.P. 168 °C; FT-IR ν (cm^{-1}): 2935 (NH), 1617 (C=N), 1440 (C−O), 652 (M−O), 555 (M−N). UV−vis (ethanol): λ_{max} 353 nm. HRMS (ESI): m/z $[M+ H]^+$ calculated for $C_{32}H_{32}Cl_4CoN_4O_2$: 706.0085, found: 706.0078.

4.3.6. Bis(4-chloro-2-((E)-(2-(4-cyanophenyl)hydrazono)-methyl)phenoxy)copper Dehydrate (1b). Yield, 62%; yellow powder; M.P. 281 °C; FT-IR ν (cm^{-1}): 3263 (NH), 1604(C=N), 1425 (C−O), 641 (M−O), 542 (M−N). UV−vis (ethanol): λ_{max} 359 nm. HRMS (ESI): m/z $[M+ H]^+$ calculated for $C_{32}H_{32}Cl_4CoN_4O_2$: 676.8580, found: 676.8579 amu.

4.3.7. Bis(4-chloro-2-((E)-(2-(4-cyanophenyl)hydrazono)-methyl)phenoxy)nickel Dehydrate (2b). Yield, 64%; light yellow powder; M.P. 284 °C; FT-IR ν (cm^{-1}): 3296 (NH), 1613 (C=N), 1276 (C−O), 626 (M−O), 542 (M−N). UV−vis (ethanol): λ_{max} 357 nm. HRMS (ESI): m/z $[M+ H]^+$ calculated for $C_{32}H_{32}Cl_4CoN_4O_2$: 672.0050, found: 672.0049.

4.3.8. Bis(4-chloro-2-((E)-(2-(4-cyanophenyl)hydrazono)-methyl)phenoxy)cobalt Dehydrate (3b). Yield, 65%; pale yellow powder; M.P. 282 °C; FT-IR ν (cm^{-1}): 3242 (NH), 1600 (C=N), 1202 (C−O), 588 (M−O), 540 (M−N). UV−vis (ethanol): λ_{max} 358 nm. HRMS (ESI): m/z $[M+ H]^+$ calculated for $C_{32}H_{32}Cl_4CoN_4O_2$: 672.2373, found: 672.2363.

4.4. Computational Analysis. All the quantum chemistry calculations were performed by using DFT implemented in the Gaussian 09 software package.[55] The geometry was optimized using the DFT approximation at the B3LYP level with a basis set of 6-31G (d, p). The improved geometries' stability was verified using frequency analysis based on the DFT/B3LYP/6-31G (d, p) level of theory. The B3LYP/6-311G (d, p) theoretical level was used for the NBO calculation. Gauss View 6[56] was utilized for the file organization of the input data. Gauss View 6.0, Avogadro,[57] and Chemcraft[58] were used to figure out the data.

4.5. Antimicrobial Activity. The antimicrobial and antifungal activities were evaluated using the already employed procedures. The synthesized compounds were tested against two Gram-negative bacteria (*Salmonella* and *E. coli*), two Gram-positive bacteria (*B. halodurans* and *M. luteus*), and two fungal strains (*A. flavus* and *A. niger*). The antibacterial and antifungal activities of the synthesized compounds were checked by the disc diffusion method.[59] Tested compounds were dissolved in a methanol solvent. A known volume (10 mL) of the prepared solution was applied on a filter paper disc with the help of a pipet, and the disc was dried overnight at room temperature. The prepared disc was placed on test bacterial strain discs, and the discs were incubated at 37 °C for 24 h. The activity was

determined by measuring the diameter of inhibition zones, which showed complete inhibition (mm).

■ ASSOCIATED CONTENT

ⓢ Supporting Information

The Supporting Information is available free of charge at https://pubs.acs.org/doi/10.1021/acsomega.3c05322.

Computation details and IR and NMR spectra (PDF)

■ AUTHOR INFORMATION

Corresponding Authors

    Riaz Hussain − *Department of Chemistry, The Education University Lahore D.G Khan campus, Dera Ghazi Khan 32200, Pakistan;* ⓞ orcid.org/0000-0002-6154-1244; Email: riaz.hussain@ue.edu.pk

    Bakhat Ali − *Institute of Chemistry, Khwaja Fareed University of Engineering & Information Technology, Rahim Yar Khan 64200, Pakistan;* Email: bakhatali@gmail.com

Authors

    Syed Laila Rubab − *Department of Chemistry, The Education University Lahore D.G Khan campus, Dera Ghazi Khan 32200, Pakistan*

    Afifa Maryam − *Institute of Chemistry, Khwaja Fareed University of Engineering & Information Technology, Rahim Yar Khan 64200, Pakistan*

    Tuba Ashraf − *Institute of Chemistry, Khwaja Fareed University of Engineering & Information Technology, Rahim Yar Khan 64200, Pakistan*

    Muhammad Arshad − *Department of Chemical Engineering, College of Engineering, King Khalid University, Abha 62529, Saudi Arabia*

    Kiran Lal − *Department of Chemistry, The Women University Multan, Multan 60000, Pakistan*

    Sajjad H. Sumrra − *Department of Chemistry, University of Gujrat, Gujrat 50700, Pakistan;* ⓞ orcid.org/0000-0002-1581-5451

    Shafaq Ashraf − *Institute of Chemistry, Khwaja Fareed University of Engineering & Information Technology, Rahim Yar Khan 64200, Pakistan*

Complete contact information is available at:
https://pubs.acs.org/10.1021/acsomega.3c05322

Notes

The authors declare no competing financial interest.

■ REFERENCES

(1) Bocian, A.; Gorczyński, A.; Marcinkowski, D.; Witomska, S.; Kubicki, M.; Mech, P.; Bogunia, M.; Brzeski, J.; Makowski, M.; Pawluć, P. New benzothiazole based copper (II) hydrazone Schiff base complexes for selective and environmentally friendly oxidation of benzylic alcohols: The importance of the bimetallic species tuned by the choice of the counterion. *J. Mol. Liq.* **2020**, *302*, No. 112590.

(2) Fouad, R. Synthesis and characterization of lanthanide complexes as potential therapeutic agents. *J. Coord. Chem.* **2020**, *73* (14), 2015−2028.

(3) Ali, B.; Stefani, H. A.; Imran, M.; Irfan, A.; Assiri, M. A.; Felinto, M. C. F.; Khalid, M.; Al-Sehemi, A. G. Synthesis, Structure Study, First-Principles Investigations and Luminescence Properties of Europium and Terbium Complexes. *J. Fluoresc.* **2020**, *30* (6), 1345−1355.

(4) Hossain, M. S.; Roy, P. K.; Ali, R.; Zakaria, C.; Kudrat-E-Zahan, M. Selected Pharmacological Applications of 1 st Row Transition Metal Complexes: A review. *Clin. Med. Res.h* **2017**, *6*, 177−191. Sumrra, S. H.; Sahrish, I.; Raza, M. A.; Ahmad, Z.; Zafar, M. N.; Chohan, Z. H.; Khalid, M.; Ahmed, S. Efficient synthesis, characterization, and in vitro bactericidal studies of unsymmetrically substituted triazole-derived Schiff base ligand and its transition metal complexes. *Monatshefte für Chemie-Chemical Monthly* **2020**, *151* (4), 549−557.

(5) Suvarapu, L. N.; Seo, Y. K.; Baek, S.-O.; Ammireddy, V. R. Review on analytical and biological applications of hydrazones and their metal complexes. *E-Journal of Chemistry* **2012**, *9* (3), 1288−1304. Shebl, M.; Khalil, S. M.; Kishk, M. A.; El-Mekkawi, D. M.; Saif, M. New less toxic zeolite-encapsulated Cu (II) complex nanomaterial for dual applications in biomedical field and wastewater remediation. *Appl. Organomet. Chem.* **2019**, *33* (10), No. e5147.

(6) Shakdofa, M. M.; Shtaiwi, M. H.; Morsy, N.; Abdel-rassel, T. Metal complexes of hydrazones and their biological, analytical and catalytic applications: A review. *Main Group Chemistry* **2014**, *13* (3), 187−218.

(7) Ashraf, T.; Ali, B.; Qayyum, H.; Haroone, M. S.; Shabbir, G. Pharmacological aspects of schiff base metal complexes: A critical review. *Inorg. Chem. Commun.* **2023**, *150*, No. 110449.

(8) Kumar, B.; Devi, J.; Manuja, A. Synthesis, structure elucidation, antioxidant, antimicrobial, anti-inflammatory and molecular docking studies of transition metal (II) complexes derived from heterocyclic Schiff base ligands. *Res. Chem. Intermed.* **2023**, *49* (6), 2455−2493.

(9) Nocheva, H.; Vladimirova, S.; Tzankova, D.; Peikova, L.; Georgieva, M. Analgesic properties of newly synthesized N pyrrolyl hydrazide hydrazones. *Tropical Journal of Pharmaceutical Research* **2023**, *22* (1), 121−127.

(10) Devi, J.; Kumar, S.; Kumar, D.; Jindal, D. K.; Poornachandra, Y. Synthesis, characterization, in vitro antimicrobial and cytotoxic evaluation of Co (II), Ni (II), Cu (II) and Zn (II) complexes derived from bidentate hydrazones. *Res. Chem. Intermed.* **2022**, 1−33.

(11) El-Sherif, A. A.; Mahmoud, W. H.; Hosny, W. M.; Komyha, E. M. Design, Structural characterization, Molecular docking, and biomedical applications of hydrazone-based Schiff base metal complexes. *Egypt. J. Chem.* **2023**, DOI: 10.21608/EJ-CHEM.2023.147796.6650

(12) Devi, J.; Kumar, B.; Taxak, B. Recent advancements of organotin (IV) complexes derived from hydrazone and thiosemicarbazone ligands as potential anticancer agents. *Inorg. Chem. Commun.* **2022**, *139*, No. 109208.

(13) Nongpiur, C. G. L.; Diengdoh, D. F.; Nagar, N.; Poluri, K. M.; Gannon, P. M.; Kaminsky, W.; Kollipara, M. R. Mono and dinuclear ruthenium, rhodium and iridium metal complexes containing N-acylhydrazone moiety: Synthesis and in vitro biological studies. *Polyhedron* **2022**, *221*, No. 115855.

(14) Alhakimi, A. N.; Shakdofa, M. M.; Saeed, S.; Shakdofa, A. M.; Al-Fakeh, M. S.; Abdu, A. M.; Alhagri, I. A. Transition Metal Complexes Derived from 2-hydroxy-4-(p-tolyldiazenyl) benzylidene)-2-(p-tolylamino) acetohydrazide Synthesis, Structural Characterization, and Biological Activities. *J. Korean Chem. Soc.* **2021**, *65* (2), 93−105.

(15) Sharma, P.; Sharma, D.; Sharma, A.; Saini, N.; Goyal, R.; Ola, M.; Chawla, R.; Thakur, V. Hydrazone comprising compounds as promising anti-infective agents: chemistry and structure-property relationship. *Materials Today Chemistry* **2020**, *18*, No. 100349.

(16) Subbiah, K.; Lee, H.-S.; Al-Hadeethi, M. R.; Park, T.; Lgaz, H. Assessment of the inhibitive performance of a hydrazone derivative for steel rebar in a simulated concrete medium: Establishing the inhibition mechanism at an experimental and theoretical level. *Chemical Engineering Journal* **2023**, *458*, No. 141347.

(17) Tokalı, F. S.; Taslimi, P.; Sadeghian, N.; Taskin-To, T.; Gülçin, İ. Synthesis, characterization, bioactivity impacts of new anthranilic acid hydrazones containing aryl sulfonate moiety as fenamate isosteres. *ChemistrySelect* **2023**, *8* (13), No. e202300241.

(18) Wang, G.; Zhang, J.; Hu, L.; Wang, J.; Zhu, C. Polydentate hydrazones as multitasking catalysts in visible-light-induced coupling reactions of amines. *Org. Biomol. Chem.* **2023**, 754 DOI: 10.1039/D2OB02092K.

(19) Suharman, S.; Hardiyanti, R. An azo/hydrazone-based chemosensor for anion detection in acetonitrile: Synthesis and spectroscopic study. In *AIP Conference Proceedings*, 2023; AIP Publishing: Vol. *2626*.

(20) Dewangan, S.; Mishra, A.; Halder, B.; Mishra, A.; Dhiman, R.; Chatterjee, S. Unsymmetrically bi-functionalized 1, 1′-ferrocenyl bi-hydrazone and hydrazone-cyanovinyl molecules as fluorescent "on−off" sensor: Synthesis, cytotoxicity and cancer cell imaging behavior. *Inorg. Chim. Acta* **2023**, *552*, No. 121511.

(21) Sumrra, S. H.; Ibrahim, M.; Ambreen, S.; Imran, M.; Danish, M.; Rehmani, F. S. Synthesis, spectral characterization, and biological evaluation of transition metal complexes of bidentate N, O donor Schiff bases. *Bioinorg. Chem. Appl.* **2014**, *2014* 812924 DOI: 10.1155/2014/812924 Sumrra, S. H.; Ibrahim, M.; Ambreen, S.; Imran, M.; Zafar, M. N.; Nazar, M. F.; Rehmani, F. S. Design, Synthesis, Spectral Characterization and Antimicrobial Studies of Metals Based Nitrogen Donor Schiff Bases. *J. Drug Des. Med. Chem.* **2016**, *2* (3), 26.

(22) Ali, A.; Khalid, M.; Abid, S.; Iqbal, J.; Tahir, M. N.; Rauf Raza, A.; Zukerman-Schpector, J.; Paixão, M. W. Facile synthesis, crystal growth, characterization and computational study of new pyridine-based halogenated hydrazones: Unveiling the stabilization behavior in terms of noncovalent interactions. *Appl. Organomet. Chem.* **2020**, *34* (3), No. e5399. Iscen, A.; Brue, C. R.; Roberts, K. F.; Kim, J.; Schatz, G. C.; Meade, T. J. Inhibition of amyloid-β aggregation by cobalt (III) Schiff base complexes: a computational and experimental approach. *J. Am. Chem. Soc.* **2019**, *141* (42), 16685−16695.

(23) Frei, A.; Verderosa, A. D.; Elliott, A. G.; Zuegg, J.; Blaskovich, M. A. Metals to combat antimicrobial resistance. *Nature Reviews Chemistry* **2023**, *7* (3), 202−224.

(24) Wehbe, M.; Leung, A. W.; Abrams, M. J.; Orvig, C.; Bally, M. B. A Perspective−can copper complexes be developed as a novel class of therapeutics? *Dalton Transactions* **2017**, *46* (33), 10758−10773.

(25) Jiménez-Pérez, V. M.; García-López, M. C.; Munoz-Flores, B. M.; Chan-Navarro, R.; Berrones-Reyes, J. C.; Dias, H. R.; Moggio, I.; Arias, E.; Serrano-Mireles, J. A.; Chavez-Reyes, A. New application of fluorescent organotin compounds derived from Schiff bases: synthesis, X-ray structures, photophysical properties, cytotoxicity and fluorescent bioimaging. *J. Mater. Chem. B* **2015**, *3* (28), 5731−5745.

(26) Manjunatha, K.; Supriya, S.; Nawaz, S. S.; Ranjan, P.; Chakraborty, T.; Poornesh, P.; Dileep, R. Nonlinear optical and quantum chemical studies of Palladium benzimidazole Schiff base complex. *Mater. Sci. Semicond. Process.* **2022**, *151*, No. 107012.

(27) Bullo, S.; Jawaria, R.; Faiz, I.; Shafiq, I.; Khalid, M.; Asghar, M. A.; Baby, R.; Orfali, R.; Perveen, S. Efficient Synthesis, Spectroscopic Characterization, and Nonlinear Optical Properties of Novel Salicylaldehyde-Based Thiosemicarbazones: Experimental and Theoretical Studies. *ACS omega* **2023**, *8* (15), 13982−13992. Khalid, M.; Jawaria, R.; Khan, M. U.; Braga, A. A. C.; Shafiq, Z.; Imran, M.; Zafar, H. M. A.; Irfan, A. An efficient synthesis, spectroscopic characterization, and optical nonlinearity response of novel salicylaldehyde thiosemicarbazone derivatives. *ACS omega* **2021**, *6* (24), 16058−16065.

(28) Rezvana, V. H.; Aminivandb, Y. DFT computational study of optical properties for bis-Schiff bases of 8-aminoquinoline derivatives and furan-2, 3-di-carbaldehyde.

(29) Niu, R.; Chen, S.; Zhou, W.; Wu, X.; Yang, J.; Wang, Y.; Zhang, X.; Song, Y. Investigation of ultrafast broadband optical nonlinearity and intensity-dependent nonlinear absorption in novel hydrazone derivatives. *Optics & Laser Technology* **2022**, *149*, No. 107798.

(30) Maharramov, A. M.; Mahmudov, K. T.; Kopylovich, M. N.; Pombeiro, A. J. *Non-covalent interactions in the synthesis and design of new compounds*; John Wiley & Sons, 2016.

(31) Singh, I.; Al-Wahaibi, L. H.; Srivastava, R.; Prasad, O.; Pathak, S. K.; Kumar, S.; Parveen, S.; Banerjee, M.; El-Emam, A. A.; Sinha, L. DFT study on the electronic properties, spectroscopic profile, and biological activity of 2-Amino-5-trifluoromethyl-1, 3, 4-thiadiazole with anticancer properties. *ACS omega* 2020, 5 (46), 30073−30087.

(32) Fahim, A. M.; Elshikh, M. S.; Darwish, N. M. Synthesis, antitumor activity, molecular docking and DFT study of novel pyrimidiopyrazole derivatives. *Current computer-aided drug design* 2020, 16 (4), 486−499.

(33) Amanullah; Ali, U.; Ans, M.; Iqbal, J.; Iqbal, M. A.; Shoaib, M. Benchmark study of benzamide derivatives and four novel theoretically designed (L1, L2, L3, and L4) ligands and evaluation of their biological properties by DFT approaches. *J. Mol. Model.* 2019, 25, 233.

(34) Kim, K. H.; Han, Y.-K.; Jung, J. Basis set effects on relative energies and HOMO−LUMO energy gaps of fullerene C36. *Theor. Chem. Acc.* 2005, 113 (4), 233−237.

(35) Okulik, N.; Jubert, A. H. Theoretical study on the structure and reactive sites of non-steroidal anti-inflammatory drugs. *Journal of Molecular Structure: THEOCHEM* 2004, 682 (1−3), 55−62.

(36) Muthu, S.; Prabhakaran, A. Vibrational spectroscopic study and NBO analysis on tranexamic acid using DFT method. *Spectrochimica Acta Part A: Molecular and Biomolecular Spectroscopy* 2014, 129, 184−192.

(37) Mahalakshmi, G.; Balachandran, V. NBO, HOMO, LUMO analysis and vibrational spectra (FTIR and FT Raman) of 1-Amino 4-methylpiperazine using ab initio HF and DFT methods. *Spectrochimica Acta Part A: Molecular and Biomolecular Spectroscopy* 2015, 135, 321−334.

(38) Parr, R. G.; Szentpály, L. v.; Liu, S. Electrophilicity index. *J. Am. Chem. Soc.* 1999, 121 (9), 1922−1924.

(39) Parthasarathi, R.; Padmanabhan, J.; Elango, M.; Subramanian, V.; Chattaraj, P. Intermolecular reactivity through the generalized philicity concept. *Chemical physics letters* 2004, 394 (4−6), 225−230.

(40) Parthasarathi, R.; Padmanabhan, J.; Subramanian, V.; Maiti, B.; Chattaraj, P. Toxicity analysis of 33′ 44′ 5-pentachloro biphenyl through chemical reactivity and selectivity profiles. *Curr. Sci.* 2004, 535−542.

(41) Glendening, E. D.; Landis, C. R.; Weinhold, F. Natural bond orbital methods. *Wiley interdisciplinary reviews: computational molecular science* 2012, 2 (1), 1−42.

(42) Szafran, M.; Komasa, A.; Bartoszak-Adamska, E. Crystal and molecular structure of 4-carboxypiperidinium chloride (4-piperidine-carboxylic acid hydrochloride). *J. Mol. Struct.* 2007, 827 (1−3), 101−107.

(43) James, C.; Raj, A. A.; Reghunathan, R.; Jayakumar, V.; Joe, I. H. Structural conformation and vibrational spectroscopic studies of 2, 6-bis (p-N, N-dimethyl benzylidene) cyclohexanone using density functional theory. *Journal of Raman Spectroscopy: An International Journal for Original Work in all Aspects of Raman Spectroscopy, Including Higher Order Processes, and also Brillouin and Rayleigh Scattering* 2006, 37 (12), 1381−1392.

(44) Snehalatha, M.; Ravikumar, C.; Joe, I. H.; Sekar, N.; Jayakumar, V. Spectroscopic analysis and DFT calculations of a food additive Carmoisine. *Spectrochim. Acta, Part A* 2009, 72 (3), 654−662.

(45) Abdelrheem, D. A.; Rahman, A. A.; Elsayed, K. N.; Abd El-Mageed, H.; Mohamed, H. S.; Ahmed, S. A. Isolation, characterization, in vitro anticancer activity, dft calculations, molecular docking, bioactivity score, drug-likeness and admet studies of eight phytoconstituents from brown alga sargassum platycarpum. *Journal of molecular structure* 2021, 1225, No. 129245.

(46) Eswaramoorthy, R.; Hailekiros, H.; Kedir, F.; Endale, M. In silico molecular docking, DFT analysis and ADMET studies of carbazole alkaloid and coumarins from roots of clausena anisata: a potent inhibitor for quorum sensing. *Adv. Appl. Bioinf. Chem.* 2021, 13−24.

(47) Das, P.; Majumder, R.; Mandal, M.; Basak, P. In-Silico approach for identification of effective and stable inhibitors for COVID-19 main protease (Mpro) from flavonoid based phytochemical constituents of Calendula officinalis. *J. Biomol. Struct. Dyn.* 2021, 39 (16), 6265−6280.

(48) Lipinski, C. A.; Lombardo, F.; Dominy, B. W.; Feeney, P. J. Experimental and computational approaches to estimate solubility and permeability in drug discovery and development settings. *Advanced drug delivery reviews* 1997, 23 (1−3), 3−25.

(49) Kumar, B.; Devi, J.; Dubey, A.; Tufail, A.; Taxak, B. Investigation of antituberculosis, antimicrobial, anti-inflammatory efficacies of newly synthesized transition metal (II) complexes of hydrazone ligands: structural elucidation and theoretical studies. *Sci. Rep.* 2023, 13 (1), 15906.

(50) Boora, A.; Devi, J.; Rom, T.; Paul, A. K. Synthesis, characterization, single crystal structure, biological evaluation of ONO donor hydrazones and their diorganotin (IV) complexes. *J. Mol. Struct.* 2023, 1284, No. 135386.

(51) Tümer, M.; Köksal, H.; Sener, M. K.; Serin, S. Antimicrobial activity studies of the binuclear metal complexes derived from tridentate Schiff base ligands. *Transition Metal Chemistry* 1999, 24 (4), 414−420.

(52) Dawar, N.; Devi, J.; Kumar, B.; Dubey, A. Synthesis, characterization, pharmacological screening, molecular docking, DFT, MESP, ADMET studies of transition metal (II) chelates of bidentate schiff base ligand. *Inorg. Chem. Commun.* 2023, 151, No. 110567.

(53) Rani, M.; Devi, J.; Kumar, B. Thiosemicarbazones-based Co (II), Ni (II), Cu (II) and Zn (II) complexes: synthesis, structural elucidation, biological activities and molecular docking. *Chem. Pap.* 2023, 6007−6027.

(54) Lashanizadegan, M.; Ashari, H. A.; Sarkheil, M.; Anafcheh, M.; Jahangiry, S. New Cu (II), Co (II) and Ni (II) azo-Schiff base complexes: Synthesis, characterization, catalytic oxidation of alkenes and DFT study. *Polyhedron* 2021, 200, No. 115148.

(55) Frisch, M. gaussian09. http://www.gaussian.com/ 2009.

(56) Dennington, R.; Keith, T. A.; Millam, J. M. *GaussView 6.0. 16.* Semichem Inc.: Shawnee Mission, KS, USA, 2016.

(57) Hanwell, M. D.; Curtis, D. E.; Lonie, D. C.; Vandermeersch, T.; Zurek, E.; Hutchison, G. R. Avogadro: an advanced semantic chemical editor, visualization, and analysis platform. *J. Cheminf.* 2012, 4 (1), 17.

(58) Andrienko, G. *Chemcraft-graphical software for visualization of quantum chemistry computations.* See https://www.chemcraftprog.com 2010.

(59) Rahman, A.; Choudhary, M. *WJ. Thomson-Bioassay techniques for drug development.* Harwood Academic Publishers: Australia, Amsterdam, The Netherlands, 2005.